SI Appendix

Interaction networks, ecological stability, and collective antibiotic tolerance in polymicrobial infections

Marjon G.J. de Vos, Marcin Zagorski, Alan McNally, Tobias Bollenbach

Materials and Methods

UTI isolates

Ninety-six isolates from 24 patients (thus 24 host communities) were selected from a previous study (1). Isolates were purified by dilution to extinction on CHROMagar Orientation (CHROMagar) to facilitate the separation. The genus of all isolates was confirmed by subsequent Sanger sequencing of the 16S rDNA. Only isolates with verified identity that were able to grow entirely planktonically in AUM and LB were used for the growth measurements. 24 isolates (25%) that did not meet these criteria were excluded. We continued with 72 bacterial isolates from 23 patients, including 8 remaining complete communities isolated from 8 hosts; the remaining bacterial communities from the other 15 hosts missed at least one isolate, and were therefore not complete (complete communities in Fig. 3B, SI Appendix, Fig. S5A). Clonal isolates were pinned on CHROMagar Orientation to reaffirm their identity and frozen as glycerol stocks (v/v 15% glycerol) on 96-well plates. Five specific taxa were shipped, but not included to the analysis due to difficulties reviving the stab cultures, contamination or non-planktonic growth; *Rhizobium radiobacter, Chryseobacterium indologenes, Gamella haemolysins, Aerococcus viridans, Aerococcus urinae* (these were all only present once in the shipped 96 isolates). Other taxa that were not included in the screen for the above reasons came from the genera *Enterococcus, Staphylococcus, Citrobacter, Pseudomonas, Proteus,* and *E.coli*. The isolates listed in this analysis are included in SI Appendix Table S1. The community analysis was performed on the 8 complete communities, which are also included in Table S1.

16S sequencing and phylogeny

Chromosomal DNA from the *Staphylococcus* strains was extracted by suspending a colony in 100 µL of lysis buffer (20 mM Tris-HCl at pH 8.3, 50 mM KCl, 1.5 mM MgCl, 0.5% (v/v) Tween 20, 0.45% (v/v) Nonidet P-40, 0.01% (m/v) gelatin, and 60 µg/mL proteinase K); the mixture was incubated at 55°C for 1 h, followed by 10 min at 95°C. All other isolates were lysed by taking a colony, suspending it in 50 µL Milli-Q water, and heating for 10min at 95°C prior to the PCR reaction. PCR amplification was carried out as follows: Initial denaturation at 95°C for 2 min, followed by 35 cycles each of 95°C for 30 s, 51°C for 30s and 72°C for 2 min, and a final elongation step at 72°C for 10 min, using universal 27F-16S (AGAGTTTGATCMTGGCTCAG) and 926R-16S (AAACTYAAAKGAATTGACGG) primers. Each PCR reaction used 25 µL of PCR mix containing: 1x GoTaq Buffer, 0.2 µM of each primer, 2 µL of suspended lysed isolate, 200µM of each dNTP in Milli-Q water. Sequencing of the gene products with above mentioned primers was performed at LGC Genomics and Eurofins. The amplified 16S sequences were aligned using Muscle multiple sequence alignment tool on the www.ebi.ac.uk website. The phylogenetic tree was constructed using the Clustal W tool on the same website, including distance correction.

Artificial urine medium (AUM)

A modified version of the AUM described in (2) was used. The AUM concentration was adapted to achieve planktonic growth of the UTI isolates and to minimize crystal formation in the replenished conditioned medium. The 1x medium contained bacto peptone L37 1.1 g/L (Oxoid), bacto yeast extract 6 mg/L (BD), lactic acid 1.32 mM (Roth), citric acid 2.4 mM, $NaHCO_3$ 30 mM, urea (Roth) 153 mM, uric acid 0.48 mM, creatine 8.4 mM, $CaCl_2$.2HO 0.24 mM, NaCl 108 mM , $FeSO4^{-}.7H_2O$ 0.006 mM, $MgSO_4.7H_2O$ 12 mM, $Na_2SO_4.10H_2O$ 12 mM (Roth), KH_2PO_4

8.4 mM, K_2HPO_4 8.4 mM, NH_4Cl 30 mM. The AUM medium was buffered with 0.1M PIPES (pH 6.5), and 1‰ (v/v) tritonX-100 was added to prevent clotting, biofilm formation and the deformation of the concave surface of the medium-air interface in the wells of the 96-well plate, which can disturb the OD_{600} measurement. All chemicals were from Sigma unless indicated otherwise.

Conditioned medium preparation

Isolates were grown for 48h in 40mL AUM in vented 50mL culture tubes (TPP) at 30°C and shaken at 200rpm. Cultures were centrifuged at 4,800g for 15 min at room temperature; the supernatant was filtered with 0.2µm filter tops (TPP), this is the spent medium from which the final conditioned medium is prepared. To make the final conditioned medium we mixed the AUM spent medium fraction with AUM medium, and the spent medium fraction was replenished with AUM constituents (without sodium chloride), such that the final concentration of constituents in the final "conditioned" medium ranged from 0.6x (for constituents that were consumed in the spent medium) to 1x (for constituents that were not at all consumed in the spent medium) of the concentration in AUM. The pH of the final conditioned media was kept at 6.4-6.5 by 0.1M PIPES buffer except for the medium conditioned by *Proteus mirabilis* which ranged from pH 7.3-7.8. This increased pH corresponds to *Proteus mirabilis' in vivo* behavior*;* it hydrolyses urea to carbon dioxide and ammonia, which increases the pH and generates calcium crystals and magnesium ammonium phosphate precipitates (3, 4).

Growth measurements

Each isolate was incubated for 36h in one well of a 96-well plate (non-treated transparent flat bottom, Nunc) containing 200 µL of pre-warmed medium. Cultures were inoculated using a replicator (V&P Scientific) transferring ~0.2 µL from a (thawed) overnight culture kept at −80°C (see "UTI isolates" above). The plates were incubated in an automated incubator (Liconic Storex) kept at 30°C, > 95% humidity, and shaken at 720 rpm in aerobic conditions. Optical density at 600 nm (OD_{600}) was measured every ~44 min in a plate reader (Tecan Infinite F500, 5 flashes, 10 ms settle time; filter: D600/20; Chroma). In addition, directly before each measurement, plates were shaken on a magnetic shaker (Teleshake; Thermo Scientific) at 900 rpm for 59s. A customized liquid handling robot (Tecan Freedom Evo 150) was used to automate these experiments and measure over 3,450 growth curves per 36h. The growth rate in exponential phase was quantified from the OD_{600} increase over time by a linear fit of $\log(OD_{600})$ in the range $0.022 < OD_{600} < 0.22$ for all isolates except *Enterococcus* spp; for the enterococci, the range $0.009 < OD_{600} < 0.021$ was used, as these strains typically reach a lower maximum OD_{600} in AUM (enterococci reach OD_{600} ~0.04 in AUM to ~0.1 in some conditioned media, other isolates generally reached OD_{600} values of 0.25 to 0.4; this relatively low final OD_{600} of enterococci in non-conditioned AUM corresponds to their poor growth in urine alone (3, 5)). The growth yield (maximum OD_{600} reached) was defined as the mean OD_{600} of the last four measurements. The vast majority of isolates reached stationary phase within 20 h, and the OD_{600} largely stayed constant during stationary phase. All experiments were performed in triplicate. Media evaporation from plates and edge effects were virtually undetectable. Directly after each growth experiment the wells were visually inspected for biofilm formation. Isolates that attached to the bottom of the well (observed by scratching each well with a 1 mL pipette tip), clots, or floating biofilms were discarded from the dataset. Biofilm formation occurred primarily for

specific isolates, and was genera unspecific. Each 96-well plate contained non-inoculated wells to control for contamination, either in the conditioned medium or during the inoculation procedure. Contamination was negligible.

Analysis of interactions in conditioned medium

Interactions of isolates were defined using the interaction parameter $\varepsilon=\log(N_c/N_u)$, where N_c is the growth yield in condition medium, and N_u the growth in the reference medium (1x AUM concentration). ε is positive ($\varepsilon>0$) if the growth yield (maximum OD_{600}) is higher than that of the reference; negative interactions correspond to $\varepsilon<0$. The level of growth inhibition due to complete resource overlap alone is $\varepsilon\approx\log(0.6)=-0.51$; this value corresponds to the lowest possible concentration of nutrients in the replenished medium. If an interaction is in the interaction-range from log(0.6) to just below log(1), then there is either resource overlap or the production of bacteriocins (or the like), or both. In case an interaction is lower than 0.6 than it cannot be due to resource overlap *alone* and must therefore involve additional mechanisms, such as the production of bacteriocins. The level of growth exceeding $\varepsilon=\log(1)=0$ likely points to additionally consumed resources in the conditioned medium, such as could be caused by cross-feeding on compounds in the medium produced by the isolate from which the conditioned medium was prepared. The mean of the triplicate growth measurements was used to calculate the interaction parameter. Unless stated otherwise (e.g. in the theoretical modeling of the community interactions), the conservative thresholds $\varepsilon=\log(0.8)=-0.22$ and $\varepsilon=\log(1/0.8)=\log(1.25)=0.22$ were used for scoring negative and positive interactions, respectively; 95% of the standard deviations around the mean of the triplicate measurements were within the bounds of this 20% threshold. Interactions on growth rate were scored analogously.

Lag time interactions were defined using the interaction parameter $\varepsilon_{lag}=\log(l_u/l_c)$, in which l_c is the lag time in condition medium, and l_u the lag time in the reference medium (1x AUM concentration). The lag time was defined as the length of time before an isolate reaches $OD_{600=}0.01$. ε_{lag} is positive ($\varepsilon_{lag}>0$) if the lag time is shorter in the conditioned medium compared to the lag time in the reference medium; negative interactions ($\varepsilon_{lag}<0$) correspond to a longer lag time.

Antibiotic tolerance interactions

Isolates were grown in 96-well plates in liquid cultures for 25h. The inoculation and growth procedures were identical to the protocol described above (section "Growth measurements"). The effect of conditioned medium on the action of antibiotics was assessed by scoring the growth in a concentration gradient of two clinically used antibiotics with different modes of action, trimethoprim-sulfamethoxazole and nitrofurantoin (6–8) in the presence and absence of conditioned medium. Five dilutions, with 3.5-fold decrements, and an additional no-drug control were used to determine the maximum antibiotic concentration that could sustain growth. Antibiotic tolerance interactions were scored as the difference in the number of antibiotic concentrations in which growth was observed in conditioned medium versus the AUM (1x concentration) reference. Growth of all isolates (except enterococci, see below) was scored positive if OD_{600} exceeded 0.02 within 25h; growth in *Proteus mirabilis* conditioned medium was conservatively scored positive as (OD_{600}[average last three time points])- (OD_{600}[average first three time points])>0.025 to correct for the increased crystal formation in the medium which affects OD_{600}. As enterococci reach lower final OD_{600} values (see above, section "Growth measurements"), growth was scored as positive if the

final OD_{600}>0.01. Antibiotics were added in the conditioned medium just before the start of the tolerance assay, i.e. they were absent during the growth of the donor from which the conditioned medium was produced. The highest concentration of trimethoprim-sulfamethoxazole used was 18.18 µg/mL trimethoprim in combination with 90.90 µg/mL sulfamethoxazole (this 1:5 ratio is in accordance with clinical use (9)), and 200 µg/mL for nitrofurantoin. Trimethoprim was dissolved in 98% ethanol, sulfamethoxazole in acetone, and nitrofurantoin in dimethylformamide (Roth). The effect of the solvents on growth was determined by growing all isolates in conditioned and non-conditioned medium with solvent; growth was slightly affected, but never altered the conditioned medium interaction. We used 14 donor isolates to generate conditioned medium for the antibiotic tolerance assessment; 9 of these 14 donor isolates were part of six of the eight complete communities (section UTI isolates, SI Appendix), whereas five were part of incomplete communities.

To assess the effect of neutral ('silent') interactions on antibiotic tolerance, we identified interactions between the 14 donor isolates and acceptor isolates that were neutral, i.e. between $\varepsilon=\log(0.8)=-0.22$ and $\varepsilon=\log(1.25)=0.22$, in the non-antibiotic environment. The interactions between these combinations of donors and acceptor isolates quantified in the presence of antibiotics are shown in SI Appendix Fig. S10B,C.

To investigate if the conferred drug tolerance interactions correlated with the sensitivity to the antibiotics of the acceptor isolates in the reference medium, and if the conferred tolerance effect was correlated between both antibiotics, we calculated the Pearson correlation coefficient and corresponding p-values.

To test the community effects on antibiotic resistance (SI Appendix, Fig. S10D), only the donor isolates derived from a complete community were assessed. These nine donor strains (*Enterococcus faecalis, Staphylococcus aureus, Staphylococcus heamolyticus, E. coli* (three different strains), *Klebsiella pneumonia, Enterobacter cloaca*, and *Proteus mirabilis*) derived from six of the eight complete host communities. To investigate the effect of within and between community effects, we compared the observed fraction of interactions with a certain sign (+/-/0) in the host community to an ensemble of 1,000 randomized communities of isolates derived from those six complete host communities, to calculate z-scores and respective p-values.

Co-culture experiments

Pre-cultures of individual isolates were grown overnight at 37°C in 1xAUM, and subsequently co-inoculated (in dual co-culture (SI Appendix, Fig. S2), or per community of four isolates (SI Appendix, Fig. S7)) at OD_{600}=0.001 in fresh pre-warmed (30°C or 37°C) 1xAUM medium, including 0.1M PIPES buffer. The dual co-cultures were grown for 30h in 180 µL in a 96-well plate in the plate reader at 30°C (with continuous shaking, double orbit, 600rpm). The community mixed cultures were grown for 30h in a) 180 µL in a 96-well plate in the plate reader at 30°C (with continuous shaking, double orbit, 600rpm), b) at the same instance in 5 mL in 13mL culture tubes at 37°C. After 30h the cultures were diluted resp. a) 36 times, b) 100 times, this dilution step was repeated twice, leading to three transfers. For both co-culture experiments, the number of colony forming units (CFU) were determined by plating aliquots of 30 µL (1,000-fold diluted) on CHROMagar plates and enterococcal selective agar plates (enteroselect agar, Antonides).

Spot-on-lawn assay

Half a volume of 2xAUM was added to half a volume pre-heated (~50°C) sterile demi-water-agar solution (30 g/L). Agar plates were prepared containing 25 mL AUM-agar. The top-agar, containing bacteria that will form a lawn, was prepared from a 333x diluted stationary phase culture in AUM agar solution. 10 mL of each top-agar-bacteria solution was added to each pre-prepared-plate of AUM agar. Spent media were prepared according to the protocol described above. 10 μL drops of spent medium were spotted in duplicate (dropped on agar surface, or slightly punctured agar surface) on each lawn, 10 μL drops of AUM were used as a control on each plate. Plates were assayed in duplicate. After 20h the plates were inspected for halos on the top agar-lawn. In total 131 interactions were assayed containing the taxa *Staphylococcus*, *Pseudomonas*, *Proteus* and *E.coli*, which were selected based on their negative interactions in the conditioned medium assay.

Statistical network analysis

The enrichment or depletion of single interactions or two-node subgraphs in the UTI network was quantified with respect to ensembles of randomized networks. Different randomized ensembles were used depending on the specific problem. First, when the distinction between genera was considered (single interactions in Fig. 2B, depletion of -/- and -/0 and enrichment of +/+ and +/0 for different genera) the network of interactions was randomized, conserving the number of positive and negative interactions but not the degree of separate isolates. In practice, 10,000 independent random network realizations were assembled and the resulting reference distributions of single interactions or two-node subgraphs were estimated for each genus. Note that the mean of these distributions is genus independent, but the width takes into account the number of strains from a given genus. By comparing estimates from the measured UTI interaction network with the corresponding distributions for the randomized networks, p-values (two-tailed) were calculated as the probability of having a result equal to or more extreme than the actual observation. Second, the enrichment or depletion of two-node subgraphs regardless of genera (Fig. 2C) was estimated with additional constraint imposed; specifically, the degree distribution was conserved. Again 10,000 random network realizations were generated: each network was obtained from the previous one by applying 4×(number of edges)≈8,500 edge swaps independently for random pairs of positive and negative interactions (self-interactions were excluded from the randomization and analysis). The resulting ensemble was used as a reference for quantifying the z-score (and respective p-values) of enrichment or depletion of the two-node subgraphs.

Statistical community analysis

There were 8 complete communities, isolated from 8 hosts, containing 4 isolates each (section “UTI isolates”). First, we checked if some pairs of genera occur more often than in the random scenario. As a reference, 10,000 sets with 8 independent 4-isolate communities were assembled by randomly sampling isolates from the complete communities. Using the obtained distributions, the random expectation and the corresponding p-value (two-tailed) of observing a given pair of genera in the original communities was calculated (SI Appendix, Fig. S5B). Second, we checked whether single interactions or two-node subgraphs are significantly enriched or depleted among complete communities. Again 10,000 communities were resampled from the 8 complete communities, but the genera for each community were preserved (e.g. the first community was always composed of *Enteroccocus*, *Staphylococus*,

Klebsiella, and *E. coli*, and only the corresponding strains changed). The resulting ensemble was used to calculate z-scores and corresponding p-values (two-tailed) for Fig. 3A.

Theoretical model of ecological interactions

We developed a minimal theoretical model describing the ecological interactions that occur between bacteria in a polymicrobial infection. Our model is based on established models (10, 11) of logistic growth in liquid batch culture without spatial structure. The model captures interactions that affect both growth rate and yield independently:

$$\dot{N}_j = N_j g_j \max\left(0, 1 + \sum_{j \neq k} a_{jk} N_k\right) \left(1 - \frac{N_j}{\max(0, 1 + \sum_{j \neq k} b_{jk} N_k)}\right) \qquad (1)$$

Here, N_j is the population size (number of individuals) of isolate j and g_j is its growth rate in isolation; N_j is non-dimensionalized so that $N_j = 1$ corresponds to the growth yield at carrying capacity of isolate j when grown in isolation. The matrix a_{jk} quantifies the growth rate interactions, i.e. how the growth rate of isolate j changes in the presence of isolate k (at saturating population size of the latter), relative to its growth rate in isolation g_j: e.g. $a_{jk} = 0$ means that there is no interaction, $a_{jk} = 1$ means that isolate j grows twice as fast and $a_{jk} = -1$ means that isolate j does not grow at all when isolate k is present at its carrying capacity. The latter captures e.g. competition for the same limiting nutrient. Similarly, the matrix b_{jk} quantifies the growth yield change of isolate j in the presence of isolate k, relative to the growth yield of isolate j in isolation. The first max function restricts effective growth rate to be non-negative, whereas the second one ensures that the growth yield does not become negative as a result of the interactions. For simplicity, all interactions are assumed to be additive when more than two isolates are present in the community.

If $b_{jk} \equiv 0$ the growth yield for $t \to \infty$ remains $N_j = 1$ as long as the growth rate interactions are sufficiently weak. In general, interactions can, however, lead to very low carrying capacity for the isolate j and force the system to the fixed point $N_j = 0$ for $t \to \infty$ (meaning that isolate j goes extinct). Importantly, all parameters of this model are fully constrained from our experiments. In particular, the matrices a_{jk} and b_{jk} follow directly from the experimental data shown in Fig. 2A and SI Appendix, Fig. S1. The a_{jk} were obtained from the experimentally measured growth rate interactions by simply subtracting 1 from g_c/g_u. The b_{jk} were obtained by subtracting 1 from the measured growth yield interactions N_c/N_u (section "Analysis of interactions in conditioned medium") and linearly rescaling negative b_{jk} to make N_c/N_u=0.6 result in b_{jk} = -1 (to ensure that these values consistently correspond to complete resource overlap). To mimic the regular voiding of the bladder, we further added a dilution term $-DN_j$ on the right hand side of eqn. (1); here D is the effective dilution rate. This term affects the stability properties of the system's fixed points (see main text and SI Appendix, Fig. S9).

Theoretical model solutions

The model defined in Eq. (1) is used to determine both the dynamics of the growing bacterial populations and the number of isolates in steady-state. In the first case, the forward propagation method was used, i.e. the set of n ODEs was numerically integrated, where n denotes the number of isolates in the community; in practice, the numerical solvers NDSolve and ParametricNDSolve in Mathematica 11.1 (*Wolfram*) were used. By default, the initial

population size N_j was assigned a random value from (0, 1] separately for each j (Fig. 3C; SI Appendix, Fig. S6). To determine the fixed points that correspond to stable coexistence of all species in a given community, Eq. (1) was solved for all steady states with $N_j > 0$. In practice, this reduces to finding all positive N_j that fulfill either $0 = 1 + \sum_{j \neq k} a_{jk} N_k$ or $N_j = 1 + \sum_{j \neq k} b_{jk} N_k$ for each j separately. Further, for the obtained set of steady state solutions, linear stability analysis was performed to identify only those solutions that are locally stable to fluctuations in population size. 4 out of 8 complete communities had a stable coexistence fixed point.

To investigate whether identified stable coexistence fixed points are reachable only from specific initial conditions (strain abundances N_j) or are independent of the initial N_j, we used the forward propagation method specified above. In particular, for each of the 4 communities with a stable coexistence fixed point, the population size N_j at t=96h was obtained (1,000 random realizations of initial conditions, $0 < N_j \leq 1$). We found that in two of these four communities the stable coexistence fixed point is always reached, in one community it is reached in 99.2% of the cases, and in another one in 84.1% of the cases (one isolate dies out otherwise). The coexistence fixed points are typically reached after several hours (Fig. 3C, SI Appendix, Fig. S6).

To determine the typical fraction of stable communities as a function of the number of taxa in a community, the isolates were randomly assembled into communities of with n = 2,…,8 different isolates using the 32 isolates that constitute the 8 complete communities (1,000 communities were assembled for each n). A community was considered stable when at least one stable fixed point with all isolates present was found (Fig. 3D).

Next, we studied invasion of the four complete communities at their stable coexistence fixed points. Specifically, the forward propagation method was used with four isolates present at their steady-state population size; an invader was added at a small population size of 0.01 at t=0. Each stable community (4 isolates) was tested against invasion by any of the 28 strains that were present in the remaining (stable and unstable) complete communities. The outcome of invasions was determined not later than at t=96h; in many cases of failed invasion the invading strain died out almost instantly. The different outcomes of invasion were defined depending on the number of isolates that survived with non-zero population sizes (see main text and SI Appendix, Table S3).

Finally, the model with dilution term $-DN_j$ added to Eq. (1) was solved by the forward propagation method. The steady state in SI Appendix Fig. S9 was determined after 96h using the population size corresponding to a steady-state with no dilution (D=0) as initial condition. Additionally, stability of communities as a function D was verified by simulating a series of discrete voidings (SI Appendix, Fig. S9). As a result, the same isolates persist (or die out) as in continuous approximation of voiding events.

Estimation of dilution rate

To calculate the range of dilution rates expected for individuals with healthy bladder and for those suffering from urinary retention, we made the following assumptions: (i) the post-void residual urine volume V_R is 5 mL for healthy individuals and 100 mL for those with urinary retention (12, 13); (ii) the total bladder volume V_B = 400 mL in both cases, (iii) there are n voiding events per 24h where $n=(V_L - V_R)/ (V_B - V_R)$ depends on the liquid consumption V_L (more precisely, liquid that gets to the bladder); V_L is assumed to be between 1 and 2 L (14–17).

The model in Eq. (1) assumes a continuous dilution rate D. Thus, we derive D as effective rate equivalent to a series of n discrete voidings per t=24h, that is $(V_R/V_B)^n$=exp(-Dt), which results in

$$D = \frac{-n \log(V_R/V_B)}{t} \quad (2)$$

Using the parameter estimates stated above and assuming a high liquid consumption (V_L = 2L), we obtain $D_H \approx$ 0.015 min^{-1} for healthy individuals and $D_R \approx$ 0.006 min^{-1} for those with urinary retention. In the case of lower liquid consumption (V_L = 1L), D_R is reduced to 0.003 min^{-1}. The estimated range of D between 0.003 and 0.015 is rather conservative (SI Appendix, Fig. S9); e.g. increasing V_L to 2,500 mL raises D_H to almost 0.02 min^{-1}, whereas an extremely low $V_L \approx$ 500 mL lowers D_R to 0.001 min^{-1}. In Fig. 3E and Fig. S9 the 'urinary retention' boundary (left side of the gray band) corresponds to a voiding pattern with high urine retention in the bladder (urine residual volume of 100 mL per voiding, 1 L voiding per 24h), the 'healthy bladder' boundary (right side) corresponds to a healthy bladder and voiding pattern (voiding 2L per 24h and residual volume 5 mL).

Simulation with discrete dilution

Instead of adding the continuous dilution term -DN_j to Eq. (1), we introduce voiding events explicitly as a series of n discrete dilutions over 24h by a factor of V_R/V_B, where n, V_R (post-void residual urine volume) and V_B (total bladder volume) were defined in the previous section. In particular, we fix the total bladder volume V_B = 400 mL and the liquid consumption V_L = 2L, and vary only V_R between 1.25 and 160 mL (SI Appendix, Fig. S9). Hence, the range of equivalent continuous dilution D (Eq. (2)) varies between 0.005 min^{-1} for low V_R and 0.02 min^{-1} for high V_R. Eq. (1) was solved using the forward propagation method, with the default initial conditions (N_j from (0, 1] for each j), and dilution events every 24/n hours. Due to regular dilutions, the population is always away from steady state. However, typically the dynamics of population converges to a common trajectory N_j(t) after a few dilution events (Fig. S9A). The results reported in (SI Appendix, Fig. S9B) are average population sizes that were reached at the last dilution preceding the 48h time point for 100 realizations of initial conditions. The averages are representative for almost all cases (>95%) independent of the initial conditions. Infrequently (<5%), and only for the two complete communities in which reaching stable coexistence for D = 0 is initial condition dependent, an additional isolate dies out for a given D. The results of discrete dilution simulation are consistent with stability predicted from continuous dilution rate model.

Relation of theoretical model to Lotka-Volterra-Gause model

By considering only growth yield interactions in Eq. (1) and writing explicitly the carrying capacity K_j of the isolate j the dynamics of the growing population is described by

$$\dot{N}_j = N_j g_j \left(1 - \frac{N_j}{K_j \max(0,1+\sum_{j\neq k} b_{jk} N_k)}\right) \quad (3)$$

The dynamics of the same growing population in Lotka-Volterra-Gause (LVG) (e.g. (18–20) with competing species is given by

$$\dot{N}_j = N_j g_j \left(1 - \frac{N_j + \sum_{j \neq k} \beta_{jk} N_k}{K_j}\right) \quad (4)$$

where $\beta_{jk} = -K_j b_{jk}$ describes the strength of interspecies interactions. Importantly, the condition for stable coexistence fixed point is the same in Eq. (3) and Eq. (4), namely for all j: $N_j > 0$ and $\frac{N_j}{K_j} = 1 + \sum_{j \neq k} b_{jk} N_k$. The reasoning can be extended for all fixed points with one or more isolates dying out (some N_j = 0), i.e. all such fixed points of the dynamics described by Eq. (4) are also fixed points of Eq. (3). To see that, let us consider only $N_j \geq 0$, then the 'max' term in Eq. (3) can be dropped resulting in both terms in parentheses in Eq. (3) and Eq. (4) being equal to 0 for the same combinations of N_j. Formally, the limit in which the denominator (the effective carrying capacity of isolate j) in Eq. (3) goes to 0 needs special treatment, but this limit is well defined, since when the denominator goes to 0 also N_j goes to 0.

Given the equivalence of two descriptions in terms of stability, the solutions for the case with two isolates can be obtained analytically. The possible outcomes of the dynamics of the two interacting isolates are shown in SI Appendix Fig. S8 as a function of the parameters b_{12} , b_{21}. Getting exact conditions for stability with respect to the nature of interspecies interactions (competitive, exploitive, cooperative) is a textbook exercise (e.g. (21)). Interestingly, when we consider the measured values of b_{12} , b_{21} for all possible pairwise interactions between any two isolates selected from the 8 complete communities (altogether 496 pairs of two isolates), the vast majority (91%, 451 pairs) exhibited stable coexistence, in several cases one strain died out (8%, 42 pairs), and in rare cases (<1%, 3 pairs) the isolates were predicted to have unbounded growth.

To address the question of correspondence of our full model (Eq. (1)) to the LVG model, we extend the latter by the $\max\left(0, 1 + \sum_{j \neq k} a_{jk} N_k\right)$ term. With this modification, the fraction of stably coexisting isolates is only slightly decreased (90%, 444 pairs) with respect to the fraction expected from Eq. (3). We classify the remaining 10% as destabilized (either one strain dies out, or in rare cases there is unbounded growth). Taken together, the growth yield interactions are key determinants of the stable coexistence with only slight modifications from the growth rate interactions.

Supplementary Figures

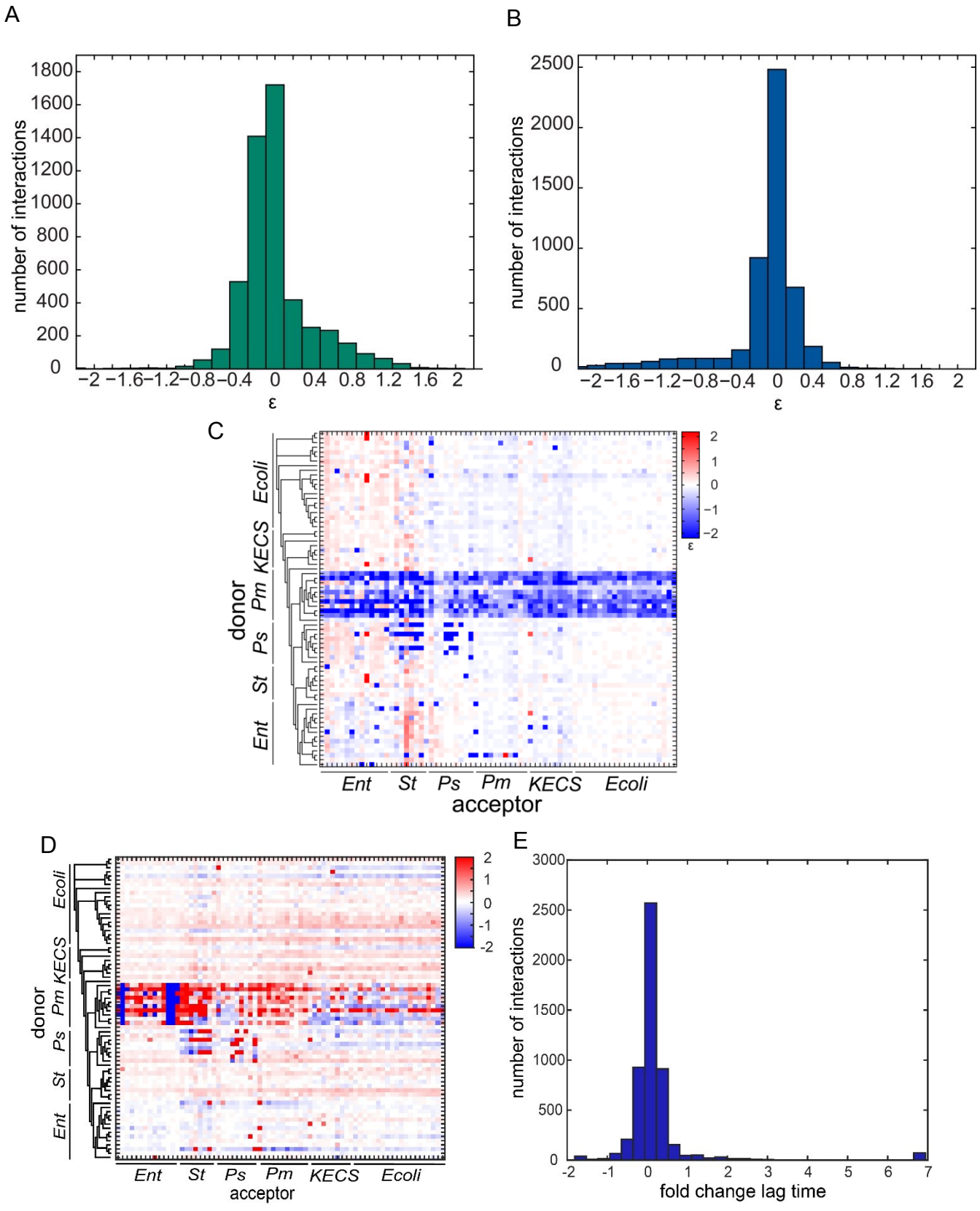

Figure S1. Growth interactions.

(**A**) Histogram of interactions between UTI bacteria affect the yield (maximum reached OD_{600}). $\varepsilon=\log(N_c/N_u)$; here, N_c and N_u are the growth yield in conditioned and in unconditioned medium, respectively. (**B**) Histogram of interactions between UTI bacteria affect the growth rate. $\varepsilon=\log(g_c/g_u)$; here, g_c and g_u are the growth rate in conditioned and in unconditioned medium, respectively. (**C**) Pair-wise interaction matrix depicting the growth rate interactions of 72 different UTI isolates in conditioned medium prepared from the same isolates. The acceptors (columns) are grown in the conditioned medium of the donors (rows). Interactions are defined as $\varepsilon=\log(g_c/g_u)$, where g_c and g_u are the growth rate in conditioned and in unconditioned medium, respectively. Interactions cluster according to phylogeny, as can be seen from the 16S rDNA phylogenetic tree on the left. The isolates are symmetrically ordered on the horizontal and vertical axes. Abbreviations as in Fig. 2. Self-interactions are on the diagonal, from bottom left to upper right. (**D**) Pair-wise interaction matrix depicting the lag interactions of 72 different UTI isolates in conditioned medium prepared from those same isolates. The acceptors (columns) are grown in the conditioned medium of the donors (rows). Interactions are defined as $\varepsilon_{lag}=\log(l_u/l_c)$, where l_u and l_c are the lag times in the unconditioned and conditioned medium, respectively, thus positive interactions correspond to shorter lag times. Interactions are ordered according to phylogeny, as can be seen from the 16S rDNA phylogenetic tree on the left. The isolates are symmetrically ordered on the horizontal and vertical axes. Abbreviations as in Fig. 2. Self-interactions are on the diagonal, from bottom left to upper right. (**E**) Histogram of effects of interactions between UTI bacteria on the lag time. Most interactions are slightly positive, meaning that the lag time is slightly shortened in conditioned medium. The main fraction (60%) of the lag interactions are between $\varepsilon_{lag}=\log(0.8)=-0.22$ and $\varepsilon=\log(1.25)=0.22$ (SI Appendix).

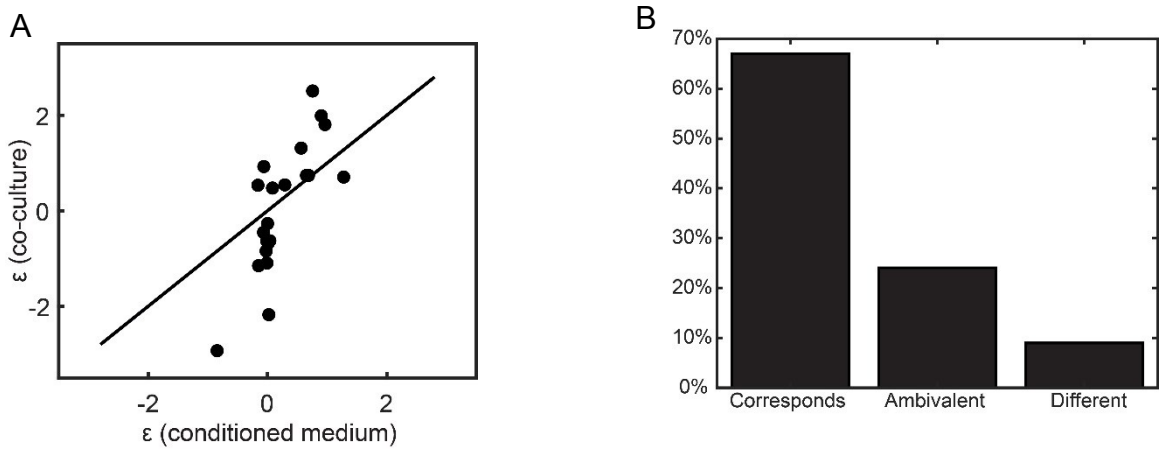

Figure S2. **Comparison of interactions assessed via co-culture, spot-on-lawn assay and conditioned medium.** (**A**) Correlation between the yield interactions in co-culture (defined as $\varepsilon=\log(CFU_{co\text{-}culture}/CFU_{isolation})$ and in conditioned medium of key taxa *E.coli, Klebsiella, Enterococus, Staphylococcus, Pseudomonas* and *Proteus*. Overall there is a strong correlation between the yield in co-culture and in conditioned medium (Pearson's $\rho=0.781$, $p<0.001$). The deviations from the diagonal line with slope 1 indicate that positive interactions of gram positives are stronger in co-culture (above line), and that gram negatives are more negatively affected in co-culture (below line) than the interactions assayed in conditioned medium. (**B**) Correspondence of spot-on-lawn assay with conditioned medium assay. Most interactions in conditioned medium correspond to those in spot-on-lawn assay. 24% of the interactions give a non-binary phenotype in the spot-on-lawn assay. These interactions show a phenotype that is different on the plate than in liquid, and could not be scored without ambivalence. For example, the addition of medium conditioned by *Proteus mirabilis* on the AUM agar plate promotes the formation of crystals, which precipitate in the AUM agar; as a result, the lawn seems to grow less dense, but spotting this medium does not clear growth completely. 9% of the interactions in the spot-on-lawn assay are qualitatively different from the conditioned medium assay. We thus conclude that the vast majority of interactions, with measured interaction parameters between $\varepsilon= \log(0.6)$ and $\varepsilon= \log(1)$, are indeed based on resource overlap and that fewer interactions, with measured interaction parameters $\varepsilon < \log(0.6)$, are due to the production of molecules like bacteriocins.

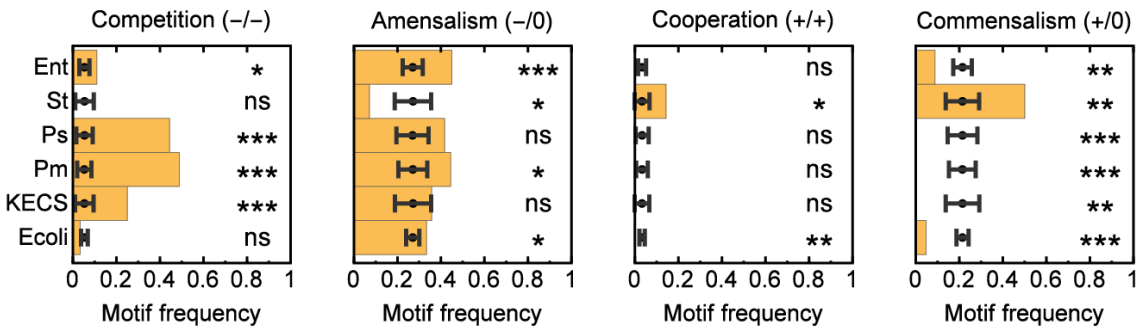

Figure S3. Over/under-representation of mutual interactions within each genus.

The frequency of mutual interactions between strains within the same genus (yellow bars) is compared with the frequency expected for a randomized interaction matrix (black dots; error bars are standard deviation). Competition and amensalism are mostly enriched while cooperation and commensalism are often depleted; *Staphylococcus* is an exception that exhibits the opposite behavior. $p > 0.05$ for "ns" (not significant), $p < 0.05$ for "*", $p < 0.01$ for "**", $p < 0.001$ for "***".

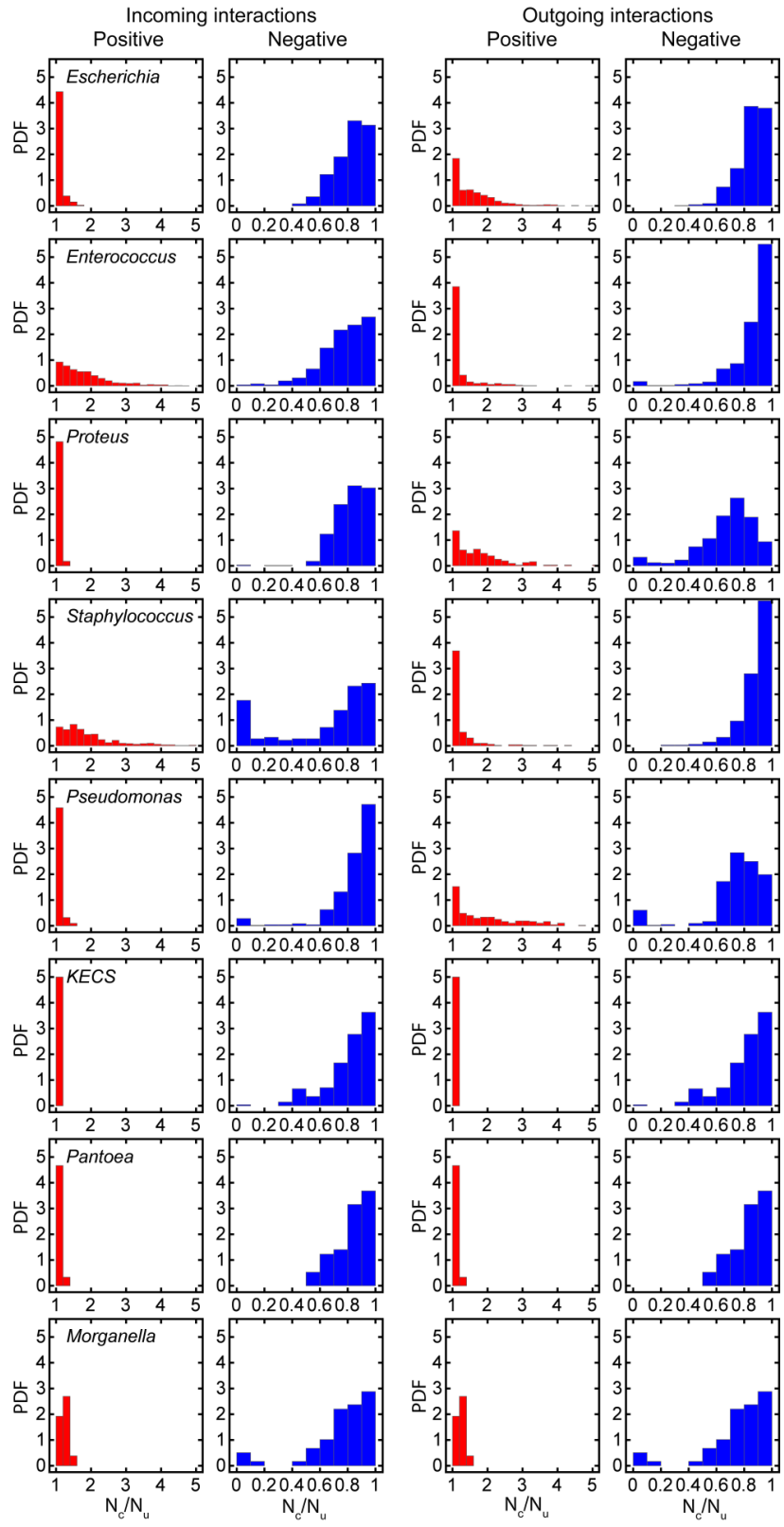

Figure S4. The strength of incoming and outgoing interactions on growth yield, ordered by genera. Incoming interactions refer to the effect from other genera (donor) on the specific genus (acceptor). Outgoing interactions refer to the effect of the specific genus (donor) on the other genera (acceptor). Negative interactions, $N_c/N_u<1$ ($\varepsilon<\log(1)$), are depicted in blue, whereas positive interactions $N_c/N_u>1$ ($\varepsilon>\log(1)$) are red.

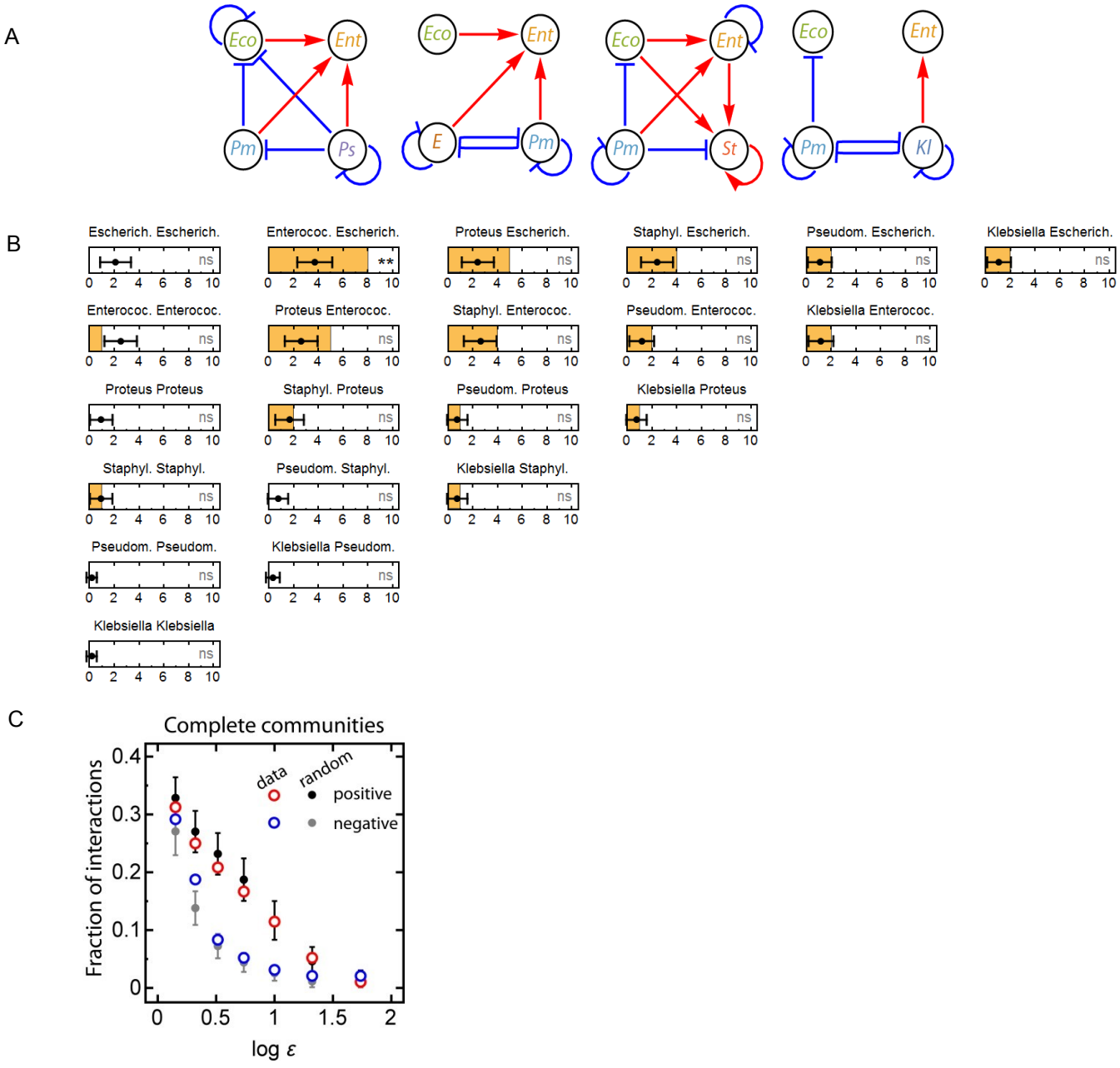

Figure S5. Interactions within UTI communities.

(**A**) Four complete unstable communities and their intra-community interactions - each depicted complete community consists of all taxa that were isolated from one host. Negative interactions (blue), positive interactions (red). Abbreviations as in Fig. 2. (**B**) The distribution of genera in each community is not random. Specifically, enterococci and *E. coli* occur more frequently together compared to an ensemble of randomly assembled communities of the same number of taxa (SI Appendix). (**C**) Communities are enriched for negative interactions, whereas postive interactions are slightly depleted. The fraction of interactions with a certain sign (red, blue) are compared to the fraction in an ensemble of randomized communities (black, gray). The x-axis shows the interaction threshold; for all further analyses the threshold level $\varepsilon=\log(0.8)=-0.22$ for negative interactions, $\varepsilon=\log(1.25)=0.22$ for positive interaction was used; error bars are standard deviations of the fraction of interactions observed in the randomized communities.

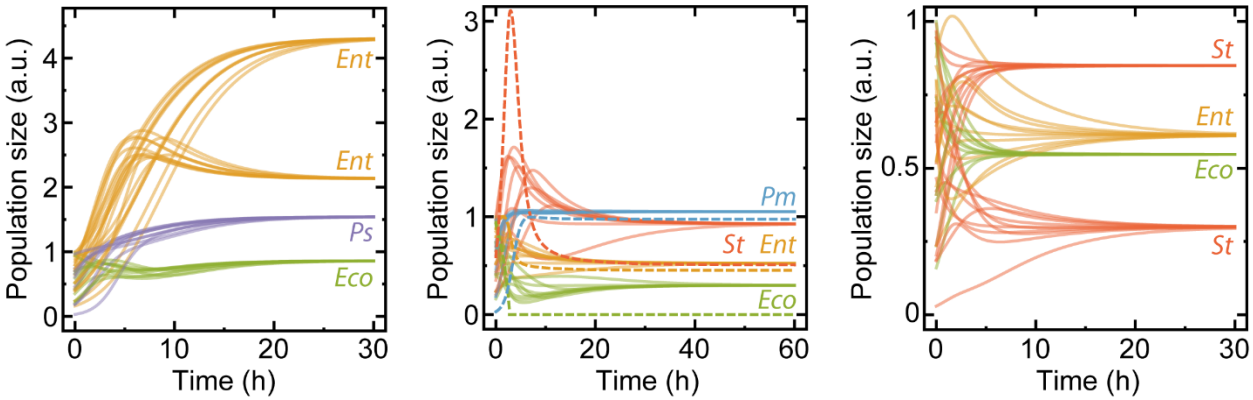

Figure S6. Communities often reach a fixed point of stable coexistence, independent of assembly order.

As Fig. 3C, but for the remaining 3 communities with a stable coexistence fixed point. In the right panel the the populations in the community reach the stable fixed point independent of initial population size (solid lines). For the middle community, most conditions (84%, SI Appendix) also lead to stable coexistence, but for the remaining 16% one of the strains dies out and only three strains coexist (dashed lines). In the community in the right panel, 99% of the conditions lead to stable coexistance. Typically the coexistence fixed point is reached within several hours. No dilution due to voiding is considered here. Abbreviations as in Fig. 2.

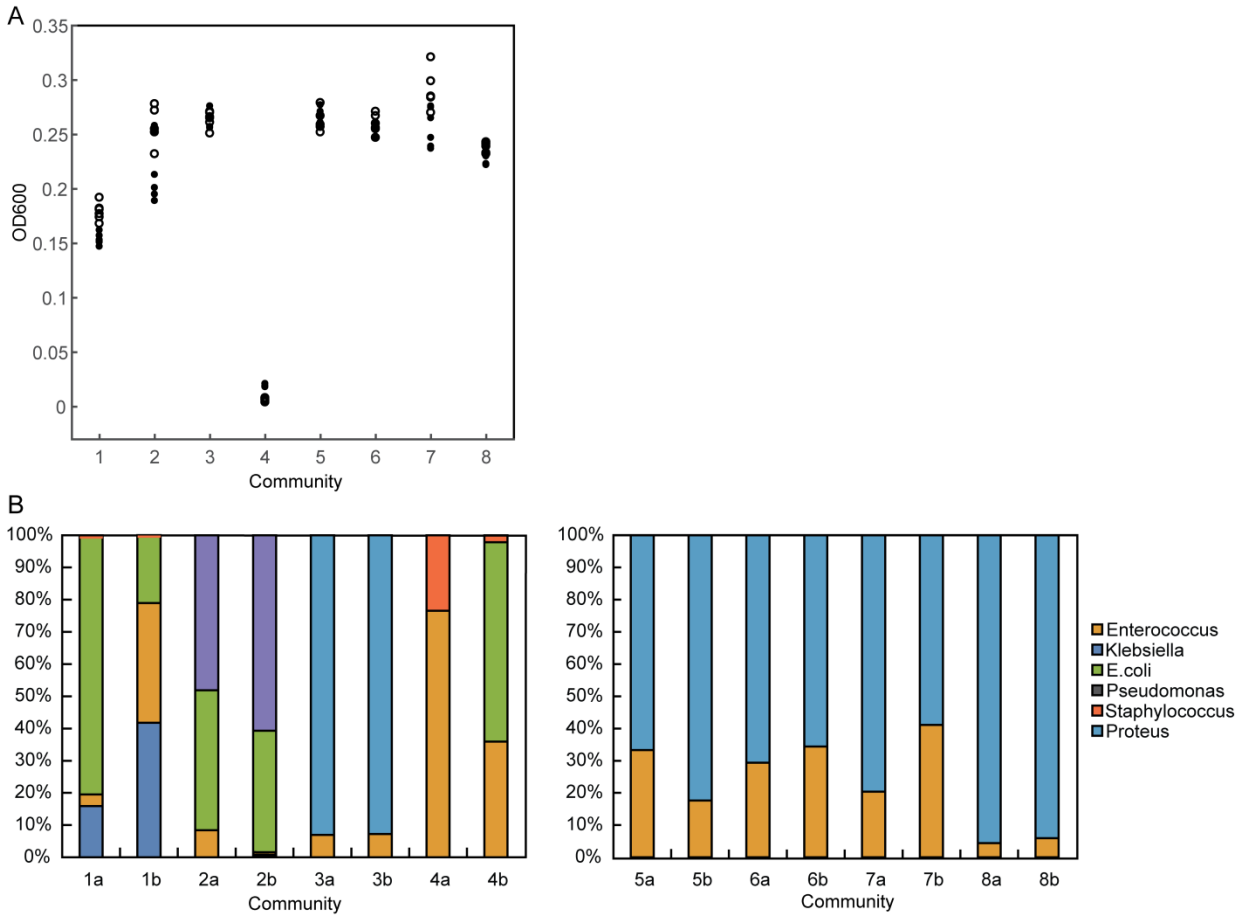

Figure S7. Community stability in *in vitro* co-culture.

(**A**) The final OD_{600} of the growth curves of the combined growth of each of the eight complete communities (Fig. 3B, SI Appendix, Fig. S5A, Table S1) is constant over transfers (closed circles second transfer, open circles third transfer, six replicates each) (SI Appendix). (**B**) The fraction of each community member in each of the eight communities (1-8, Fig. 3B, SI Appendix, Fig. S5A), at 30°C (a), 37°C (b). The left panel of B contains the communities predicted to be stable (reaching the stable fixed point in 100% (1), 100% (2), 84% (3), 99% (4) of cases, as predicted by the forward propagation method, with different initial conditions, SI Appendix), while the second panel contains the communities predicted to be unstable. Both temperatures lead to generally similar results. At 30°C two communities (1 and 2) contained all community members after three transfers (the communities predicted to be stable in 100% of the initial inocula), whereas all others communities (four predicted to be unstable, and two predicted to reach the stable fixed point from 84% and 99% of the initial conditions, respectively) only maintained two community members. In community 1, the abundance of Staphylococcus is ~1% (top of the bar graph). In communities 2a,b and 4b, there are two members of the same genus present in the community, which corresponds to the same color in the bar graph (and SI Appendix, Fig. S6, Fig. S9). At 37°C, stability was promoted further: three communities maintained all four community members (the communities predicted to reach the stable coexistence fixed point in 100% (community 1,2), resp. 99% of the initial conditions, community 4). In contrast, the communities predicted to be unstable and the community predicted to be stable in 84% of case (community 3) only contained two remaining community members (SI Appendix). Generally, the communities predicted to be stable (left panel) contained a higher diversity of species than the communities predicted to be unstable (right panel).

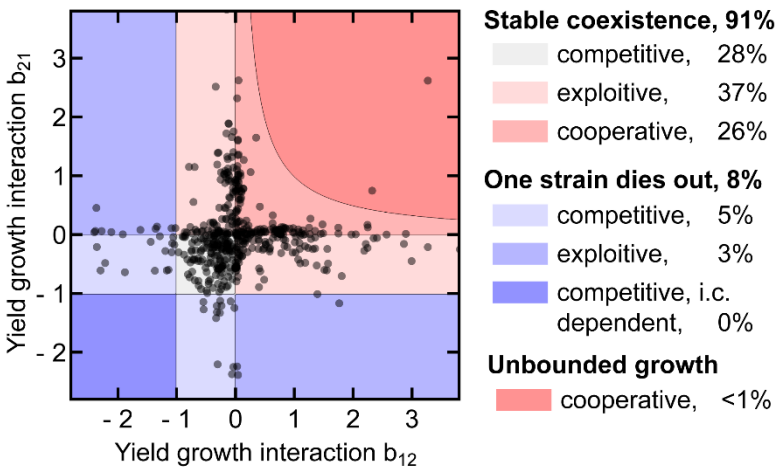

Figure S8. Phase space of possible outcomes of population dynamics with two isolates in the Lotka-Volterra-Gause (LVG) model.

The phase diagram indicates different classes of possible long-term behavior for a population of two isolates in the LVG model, Eq. (4). With respect to stability, the classes can be divided into three distinct behaviors: stable coexistence of both isolates, one of the isolates dies out, and unbounded growth. Further, the plot shows a division into subclasses depending on the sign of interactions between strains: competitive (-/-), exploitive (-/+ or +/-), or cooperative (+/+). According to the LVG model, only in the case of strong competitive interactions (b_{12} <-1, b_{21} <-1) the outcome depends on the initial size of each population ("i.c. dependent"). The dots indicate all possible pairs of isolates selected from 8 complete communities (altogether 496 pairs of isolates). The percentage indicates the fraction of pairs in the respective stability classes of the LVG model with further sub-division based on the sign of the interactions. The predicted 91% of stably coexisting pairs are in agreement with 90% of stable pairs predicted in the full model, Eq. (1), (Fig. 3D).

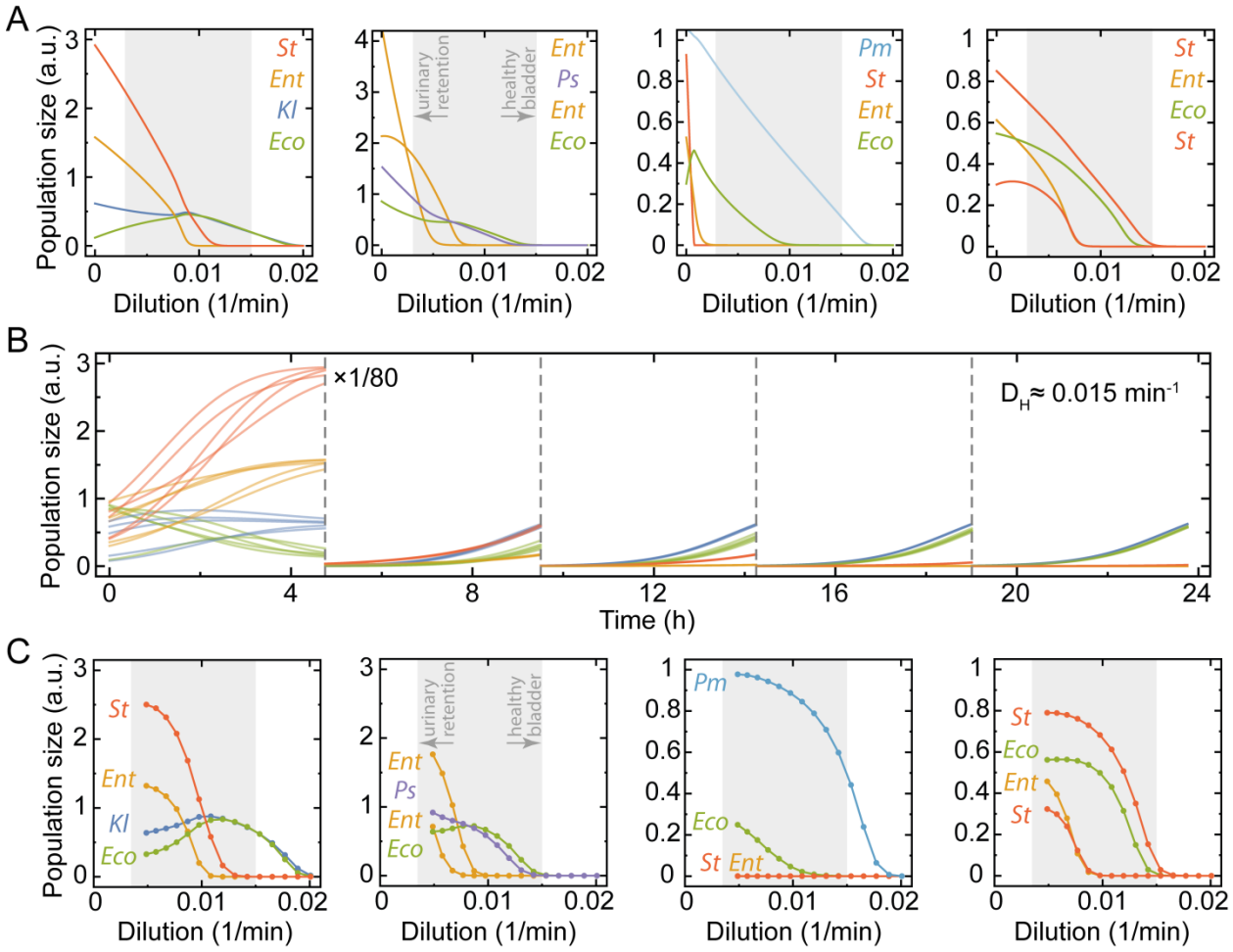

Figure S9. The stability of the UTI communities depends on the effective dilution rate.

(**A**) Steady state population size for different UTI species as a function of the effective dilution rate for all different host communities predicted to be stable (ordered in community order 1-4, including Fig. 3E for comparison).The effective dilution rate (mimicking repeated voiding of the bladder) markedly affects the stability of the community. The gray band shows the voiding patterns ranging from a healthy bladder, to a bladder with an increased post-void residual urine volume. For high effective dilution rates, all UTI community members are washed out. In the lowest dilution regime, the community constituents depend mostly on their intrinsic growth rate and yield and on the ecological interactions among the community members. In the intermediate regime, the dilution rate together with the intrinsic growth rate and yield of each isolate determines the population size of the constituents of the community. Coexistence of the species is quickly lost for increasing dilution of community 3, which corresponds to co-culture experiments. Note that *E. coli* (the main UTI pathogen in otherwise healthy persons) is consistently among the last two isolate that can still persevere at the highest dilution rates, except in community 3. (**B**) The stability of UTI dynamics in a simulation with periodic voiding events is the same as in the continuous dilution rate approximation. Example dynamics of a growing population of community 1 undergoing periodic voiding mimicking a healthy bladder. Indicated discrete dilution events (dashed lines) by a factor of 1/80 correspond to effective dilution rate of 0.015 min^{-1}, see Eq. (2) in SI Appendix. Independent of the initial population abundance, the population dynamics converges to a common behavior already after a few dilutions. (**C**) Results of periodic voiding simulation for all stable communities as a function of corresponding continuous dilution rate. Due to periodic

voiding events, the system is never at the steady state, but as dynamics converges to a common behavior we report the population size reached at the last voiding preceding 48h. The results are in agreement with continuous dilution rate approximation (panel A, SI Appendix) as the same strains persist with increasing dilution rate. The gray region is the same as in Fig. 3E and panel A.

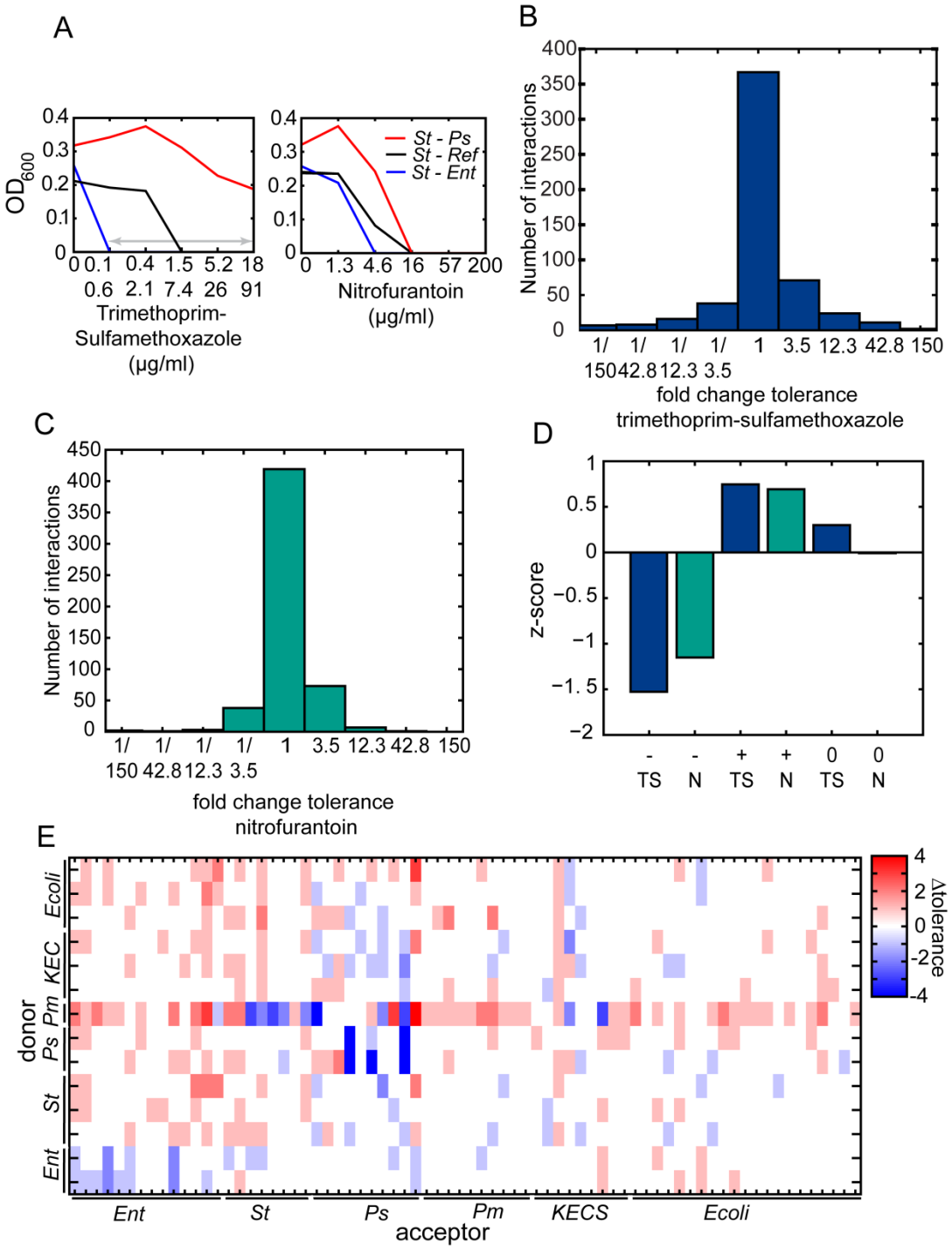

Figure S10. Bacteria in polymicrobial UTIs can protect each other from antibiotics.

(**A**) Bacterial interactions can elicit a change in the dose response curve. The dose response curves (growth yield, OD_{600}, as a function of drug concentration) of *Staphylococcus haemolyticus* for five increasing concentrations of trimethoprim-sulfamethoxazole (left) and nitrofurantoin (right) are shown in the presence and absence of conditioned medium. Black: dose response curve in reference medium (AUM); blue: medium conditioned by *Enterococcus faecalis,* red: medium conditioned by *Pseudomonas aeruginosa*. Arrows point to the change in tolerated concentration antibiotic. The increase in tolerance in conditioned medium does not always coincide with a

general growth increase in the absence of antibiotic as can be seen in these example dose response curves. (**B,C**) As Fig. 4A,B but only those interactions that are neutral in the absence of antibiotics are depicted. Interactions that are neutral (ε between log(0.8)=-0.22 and log(1.25)=0.22) in the absence of antibiotics can affect the tolerance to trimethoprim-sulfamethoxazole (left) and nitrofurantoin (right). (**D**) Enrichment or depletion of antibiotic tolerance effects within communities. TS=trimethoprim-sulfamethoxazole, N=nitrofurantoin. Interactions between isolates within the communities show a depletion of interactions that confer an increased sensitivity to the antibiotics (-), while there is a slight enrichment of protective effects (+), compared to interactions between communities. The fraction of neutral interactions on tolerance (0) does not differ within and between communities. (**E**) Interaction matrix showing the effect of conditioned medium on the tolerance to nitrofurantoin. As Fig. 4C, but for nitrofurantoin. Interaction matrix depicting the effect on the tolerance to nitrofurantoin of 14 conditioned media on 72 isolates in conditioned medium (SI Appendix). Abbreviations as in Fig. 2.

Complete communities
Comm1
Klebsiella pneumoniae
Enterococcus faecalis
Escherichia coli 1
Staphylococcus aureus
Comm2
Enterococcus faecium
Enterococcus faecium
Escherichia coli 1
Pseudomonas aeruginosa
Comm3
Enterococcus faecalis
Escherichia coli 1
Staphylococcus haemolyticus
Proteus mirabilis
Comm4
Enterococcus faecalis
Escherichia coli 1
Staphylococcus aureus
Staphylococcus simulans
Comm5
Pseudomonas aeruginosa
Enterococcus faecalis
Proteus mirabilis
Escherichia coli 1
Comm6
Enterococcus faecalis
Proteus mirabilis
Enterobacter cloacae
Escherichia coli
Comm7
Enterococcus faecalis
Escherichia coli 1
Proteus mirabilis
Staphylococcus haemolyticus
Comm8
Enterococcus faecalis
Escherichia coli 1
Klebsiella oxytoca
Proteus mirabilis

Incomplete communities
Comm9
Pseudomonas fluorescens
E. coli 1
Klebsiella pneumoniae
Chryseobacterium indologenes
Comm10
Pseudomonas aeruginosa
Enterococcus faecalis
Escherichia coli 1
Enterococcus faecalis
Comm11
Serratia liquefaciens
Citrobacter koseri
Escherichia coli 1
Staphylococcus simulans
Gemella haemolysans
Comm12
Enterococcus faecium
Pseudomonas luteola
Escherichia coli 1
Proteus mirabilis
Comm13
Pseudomonas aeruginosa
Proteus mirabilis
Escherichia coli 1
Rhizobium radiobacter
Comm14
Pseudomonas aeruginosa
Escherichia coli 1
Staphylococcus epidermidis
Pantoea spp4
Comm15
Escherichia coli 1
Enterococcus faecalis
Staphylococcus epidermidis
Pseudomonas aeruginosa
Comm16
Escherichia coli 1
Citrobacter koseri
Enterococcus faecalis
Morganella morganii

Incomplete communities
Comm17
Proteus mirabilis
Aerococcus urinae
Staphylococcus capitis
Escherichia coli 1
Comm18
Proteus mirabilis
Enterococcus faecalis
Staphylococcus aureus
Pseudomonas aeruginosa
Escherichia coli 1
Comm19
Escherichia coli 1
Enterobacter cloacae
Enterococcus faecalis
Morganella morganii
Comm20
Escherichia coli 1
Aerococcus viridans 2
Pseudomonas aeruginosa
Enterococcus faecalis
Pseudomonas aeruginosa
Comm21
Escherichia coli 1
Pseudomonas aeruginosa
Staphylococcus capitis
Enterococcus faecalis
Comm22
Proteus mirabilis
Escherichia coli 1
Enterococcus faecalis
Staphylococcus auricularis
Comm23
E. coli 1
Citrobacter braakii
Staphylococcus haemolyticus
Comm24
Proteus mirabilis
Aerococcus viridans 2
Escherichia coli 1

Table S1. Polymicrobial UTI isolates. Obtained isolates (originated from (1)) ordered according to their respective host communities. Black isolates included in this study. Gray isolates not included in this study due to either contamination during transport/ reviving procedure, non-planktonic growth in AUM or LB, or non-viable after shipping as stab culture. Communities 1 to 8 are complete; all isolates identified in the polymicrobial UTI in one host were included in this study. Communities 9-24 are incomplete, at least one of the isolates in the polymicrobial UTI community was not included in this study. Communities 1-4 are predicted to be stable, communities 5-8 are predicted to be unstable.

	Ent Ent	*St St*	*Ps Ps*	*Pm Pm*	*KECS KECS*	*Ecoli Ecoli*
0/0	-0.1134	-0.3970	-0.0102	<-0.0001	0.731	<0.0001
+/0	-0.0018	0.0014	-0.0004	<-0.0001	-0.0016	<-0.0001
+/+	-0.0892	0.0280	-0.5890	-0.4392	-0.7854	-0.0020
-/0	0.0002	-0.0156	0.0794	0.0156	0.4104	0.0498
-/-	0.0436	-0.4284	<0.0001	<0.0001	0.0004	-0.2484
+/-	0.9890	-0.6266	-0.0854	-0.0320	-0.1780	<-0.0001

Table S2. Mutual interactions within each genus. Mutual interactions are generally enriched for competition and amensalism and depleted of cooperation and commensalism; the sole exception is *Staphylococcus* which shows an enrichment of positive interactions. The values shown are p-values, negative values correspond to depletion whereas positive values correspond to enrichment (SI Appendix). Abbreviations as in Fig. 2.

Community	Coexist (5 isolates present)	Invade & replace a isolate	Fail to invade (invader dies)	Invade & destabilize (>1 get extinct)
(1)Ecoli, Ent,Kl,St	0.29	0.43	0.11	0.18
(2)Ecoli,Ent,Ent,Ps	0.68	0.04	0.29	---
(3)Ecoli,Ent,Pm,St	0.39	0.29	0.25	0.07
(4)Ecoli,Ent,St,St	0.43	0.54	---	0.04
average	0.45	0.32	0.16	0.07

Table S3. The fate of the four stable UTI communities upon invasion with a randomly chosen invader.

The most common fate of the stable communities when invaded by a randomly chosen invader is that the invader is included in the community. This new community (consisting of 4 plus 1 members) is stable. The next common fates are that one isolate is replaced by the invader, or that the invader goes extinct. In on average 7% of the cases, the invader leads to the destabilization of the community, such that more than one isolate goes extinct. Abbreviations as in Fig. 2, and Kl=*Klebsiella*.

References

1. Croxall G, et al. (2011) Increased human pathogenic potential of *Escherichia coli* from polymicrobial urinary tract infections in comparison to isolates from monomicrobial culture samples. *J Med Microbiol* 60(1):102–109.
2. Brooks T, Keevil CW (1997) A simple artificial urine for the growth of urinary pathogens. *Lett Appl Microbiol* 24(3):203–206.
3. Flores-Mireles AL, Walker JN, Caparon M, Hultgren SJ (2015) Urinary tract infections: epidemiology, mechanisms of infection and treatment options. *Nat Rev Microbiol* 13(5):269–284.
4. Armbruster CE, Mobley HLT (2012) Merging mythology and morphology: the multifaceted lifestyle of *Proteus mirabilis*. *Nat Rev Microbiol* 10(11):743–754.
5. Flores-mireles AL, Pinkner JS, Caparon MG, Hultgren SJ (2015) EbpA vaccine antibodies block binding of *Enterococcus faecalis* to fibrinogen to prevent catheter-associated bladder infection in mice. *Sci Transl Med* 6(254):1–23.
6. Gleckman R, Blagg N, Joubert DW (1981) Trimethoprim: mechanisms of action, antimicrobial activity, bacterial resistance, pharmacokinetics, adverse reactions, and therapeutic indications. *Pharmacotherapy* 1(1):14–20.
7. Hitchings GH (1973) Mechanism of action of trimethoprim-sulfamethoxazole-I. *J Infect Dis* 128(Supplement 3):S433.
8. McOsker C, Fitzpatrick P (1994) Nitrofurantoin: Mechanism of action and implications for resistance development in common uropathogens. *J Antimicrob Chemother* 33(suppl A):23–30.
9. Yoshikawa TT, Guze LB (1976) Concentrations of trimethoprim-sulfamethoxazole in blood after a single, large oral dose. *Antimicrob Agents Chemother* 10(3):462–463.
10. Tsoularis A, Wallace J (2002) Analysis of logistic growth models. *Math Biosci* 179(1):21–55.
11. Meyer PS, Ausubel JH (1999) Carrying capacity: A model with logistically varying limits. *Technol Forecast Soc Change* 61(3):209–214.
12. Kolman C, Girman CJ, Jacobsen SJ, Lieber MM (1999) Distribution of post-void residual urine volume in randomly selected men. *J Urol* 161(1):122–127.
13. Griffiths D, Harrison G, Moore K, McCracken P (1996) Variability of post-void residual urine volume in the elderly. *Urol Res* 24:23–26.
14. Martin LJ, Zieve D, Ogilvie I (2016) MedlinePlus. *Urine 24-hour volume* https://medlineplus.gov/ency/article/003425.htm.
15. Lukacz ES, et al. (2011) A healthy bladder: A consensus statement. *Int J Clin Pract* 65(10):1026–1036.
16. Walker-Smith J, Murch S (1999) *Diseases of the Small Intestine in Childhood, 4th Ed* (CRC Press).
17. Boron WF, Boulpaep EL (2016) *Medical Physiology, 3rd Ed* (Elsevier Health Sciences).
18. Gause F (1934) The Struggle for Existence. *Yale J Biol Med* 7(6):609.
19. Lotka AJ (1920) Undamped Oscillations Derived From Mass Action. *J Am Chem Soc* 42(8):1595–1599.
20. Volterra V (1926) Fluctuations in the abundance of a species considered mathematically. *Nature*

118(2972):558–560.

21. Murray JD (2002) *Mathematical Biology I. An introduction* (Springer).